



ADGB variants cause asthenozoospermia and male infertility

Ronggui Qu¹ · Zhihua Zhang¹ · Ling Wu² · Qun Li¹ · Jian Mu¹ · Lin Zhao¹ · Zheng Yan² · Wenjing Wang¹ · Yang Zeng¹ · Ruyi Liu¹ · Jie Dong¹ · Qiaoli Li¹ · Xiaoxi Sun³ · Lei Wang¹ · Qing Sang¹ · Biaobang Chen⁴ · Yanping Kuang²

Received: 9 November 2022 / Accepted: 15 March 2023

© The Author(s), under exclusive licence to Springer-Verlag GmbH Germany, part of Springer Nature 2023

Abstract

Asthenozoospermia is one of the main factors leading to male infertility, but the genetic mechanisms have not been fully elucidated. Variants in the androglobin (*ADGB*) gene were identified in an infertile male characterized by asthenozoospermia. The variants disrupted the binding of ADGB to calmodulin. *Adgb*^{-/-} male mice were infertile due to reduced sperm concentration (< 1 × 10⁶ /mL) and motility. Spermatogenesis was also abnormal, with malformation of both elongating and elongated spermatids, and there was an approximately twofold increase in apoptotic cells in the cauda epididymis. These exacerbated the decline in sperm motility. It is surprising that ICSI with testicular spermatids allows fertilization and eventually develops into blastocyst. Through mass spectrometry, we identified 42 candidate proteins that are involved in sperm assembly, flagella formation, and sperm motility interacting with ADGB. In particular, CFAP69 and SPEF2 were confirmed to bind to ADGB. Collectively, our study suggests the potential important role of *ADGB* in human fertility, revealing its relevance to spermatogenesis and infertility. This expands our knowledge of the genetic causes of asthenozoospermia and provides a theoretical basis for using *ADGB* as an underlying genetic marker for infertile males.

Introduction

Infertility has been estimated to affect approximately 15% of all reproductive-aged couples worldwide, of which 20–50% of the cases are caused by male factors, with approximately 4% having a genetic cause (Agarwal et al. 2015; Houston et al. 2021; Leaver 2016; Vander and Wyns 2018).

Asthenozoospermia is one of the common causes of male infertility and is defined as a condition in which the progressive motility rate is less than 30% (WHO 2021). Many factors, including urogenital tract infections, varicocele, flagellar anatomic defects, metabolic diseases, and genetic factors, have been found to be responsible for asthenozoospermia. Several genes have been identified as being responsible for asthenozoospermia, especially those that cause flagellar defects (Toure et al. 2021; Weng et al. 2021), such as *DNAL11* (Wu et al. 2023), *AK7* (Lores et al. 2018), and *DNAAF2* (Lu et al. 2021). Sperm flagellum are mainly composed of core axoneme, outer dense fiber, fibrous sheath, and mitochondrial sheath. All of these parts work together to maintain the structure and function of the flagellum. Variants of CFAP family members, *CFAP69* (He et al. 2019) and *CFAP43/44* (Wu et al. 2019), would lead to human multiple morphological abnormalities of the sperm flagellum

Ronggui Qu, Zhihua Zhang and Ling Wu contributed equally to this work.

✉ Qing Sang
sangqing@fudan.edu.cn
✉ Biaobang Chen
chenbiaobang@163.com
✉ Yanping Kuang
kuangyanp@126.com

¹ The Institutes of Biomedical Sciences, the State Key Laboratory of Genetic Engineering and the Institute of Pediatrics, Children's Hospital of Fudan University, Fudan University, Shanghai 200032, China

² Department of Assisted Reproduction, Shanghai Ninth People's Hospital, Shanghai Jiao Tong University School of Medicine, Shanghai 200011, China

³ Shanghai Ji Ai Genetics and IVF Institute, Obstetrics and Gynecology Hospital, Fudan University, Shanghai 200011, China

⁴ NHC Key Lab of Reproduction Regulation (Shanghai Institute for Biomedical and Pharmaceutical Technologies), Fudan University, Shanghai 200032, China

(MMAF). Axonemal dynein family genes, like *DNAH1* (Ben et al. 2014), *DNAH8* (Liu et al. 2020), and *DNAH17* (Zhang et al. 2020) were reported to contribute to male infertility in both human and mice, characterized by severe decrease in sperm motility and morphological abnormalities. AKAP3 and AKAP4 are the two main members of fibrous sheath, defect of which will decrease the motion of sperm (Miki et al. 2002; Xu et al. 2020). Genes associated with glyco-lytic enzymes or anion fluxes, such as *SLC26A8* (Gao et al. 2021), *GALNTL5* (Hagiuda et al. 2020), *ADCY10* (Akbari et al. 2019), and *CATSPER1-4* (Sun et al. 2017), have also been found to be related to asthenozoospermia. However, the genetic causes of asthenozoospermia remain to be fully elucidated.

ADGB, a chimeric globin, was first identified in 2012 (Hoogewijs et al. 2012). The protein contains an N-terminal calpain-like protease domain, a central rearranged globin domain with a calmodulin (CaM)-binding IQ motif, and a C-terminal coiled-coil region, and is highly expressed in human and mouse testes (Hoogewijs et al. 2012). *ADGB* knockdown has been observed to inhibit proliferation and increase apoptosis in glioma cell lines (Huang et al. 2014). Furthermore, Joachimiak et al. (2021) showed that in the model ciliate *Tetrahymena thermophila*, loss of *Adgb* caused minor alterations in ciliary motility. In addition, Koay et al. (2021) suggested that *FOXJ1*, a crucial transcription factor required for ciliogenesis, regulates the expression of *ADGB* and confirmed the ciliogenesis-associated role of *ADGB* in mammals. They also found that the expression of the *Adgb* transcript was restricted to stages at which round spermatids differentiate into elongating spermatids and develop a flagellum. Studies performed on infertile men with decreased expression of the *ADGB* transcript suggested its potential role in spermatogenesis (Platts et al. 2007). Although a recent study clarified the role of *Adgb* in mouse spermatogenesis (Keppner et al. 2022), there have been no reports specifying a causal relationship between *ADGB* variants and human male fertility.

In this study, we used whole-exome sequencing to find the genetic causes of individuals with asthenozoospermia and identified *ADGB* variants in an infertile male. In vitro studies showed that p.Leu426CysfsTer9 resulted in a truncated protein that could no longer interact with CaM, and p.Glu1107Ter resulted in a truncated protein with decreased protein level. Furthermore, *Adgb*^{-/-} male mice were found to be infertile owing to severe sperm head and tail deformities, and the fertilization failure could be rescued by ICSI with testicular sperm. Mass spectrometry (MS) data provided us with 42 candidates to interact with *ADGB*, from which CFAP69 and SPEF2 were selected to verify. In conclusion, this study reveals the important role of *ADGB* in male fertility and provides a novel candidate pathogenic gene responsible for the development of asthenozoospermia.

Materials and methods

Study subjects

In this study, we screened variants from a cohort of 126 male infertility patients with typical asthenozoospermia who were recruited from 2015 to 2020 from 62 collaborating hospitals and reproductive centers in China. The affected proband was recruited from the Shanghai Ninth Hospital affiliated with Shanghai Jiao Tong University. The patient had no diseases related to the reproductive system, and female factors were excluded.

Whole-exome sequencing and bioinformatic analysis

Genomic DNA was extracted from a whole peripheral blood sample using a QIAamp DNA Blood Midi Kit (Qiagen, Duesseldorf, Germany). Whole-exome sequencing was performed using an Illumina HiSeq 3000 platform (Illumina, San Diego, CA, USA), and the original data were mapped to the human genome assembly GRCh37 to detect rare novel variants. The candidates were identified in accordance with the following filtering criteria: (1) a minor allele frequency of less than 1% in the genome Aggregation Database (gnomAD); no homozygous or compound-heterozygous variants were detected in our control database, (2) missense variants were predicted to be damaging or disease-causing by SIFT, PolyPhen-2, and MutationTaster; splicing or frameshift variants were predicted to be loss-of-function, and only homozygous or compound-heterozygous variants were selected, and (3) specific expression in the testis or sperm. The variants in affected individuals were verified by Sanger sequencing.

Expression vector construction and cell transfection

The full-length coding sequence of human *ADGB* (GenBank: NM_024694.4) was purchased from FulenGen (Guangzhou, China) and cloned into a FLAG-tagged pCMV6-entry vector. The point mutation was generated using a KOD-Plus Mutagenesis Kit (Toyobo, Osaka, Japan) according to the manufacturer's protocol. Changes in protein expression levels were detected by using anti-FLAG antibody. The full-length coding sequence of human *CaM* (GenBank: NM_006888) was bought from Vigene Biosciences (Shandong, China) and cloned into a HA-tagged pCMV6-entry vector. Wild-type (WT) and mutant plasmids of *ADGB* or *CaM* expression plasmid were transfected into HEK 293T cells using a PolyJetTM DNA In Vitro Transfection Reagent (SignaGen Laboratories, Rockville, MD, USA).

Western-blot and co-immunoprecipitation

To determine the levels of protein, cells were lysed 36–40 h after transfection in RIPA lysis buffer (WellBio, Shanghai, China) supplemented with a 1% protease inhibitor cocktail (Bimake, Houston, TX, USA). The lysate was centrifuged at 12,000×*g* for 15–20 min at 4 °C, and the protein concentration in the supernatant was measured using the bicinchoninic acid method, after which equal amounts of protein components were separated on 10% SDS-PAGE gels. Thereafter, the proteins were transferred onto nitrocellulose membranes (PALL Corporation, NY, USA) and then blocked with 5% non-fat milk for 1 h. The membranes were then incubated overnight with anti-FLAG antibody (1:3,000 dilution, 2368; Cell Signaling Technology, Danvers, MA, USA) at 4 °C, or Vinculin (anti-Vinculin; 1:3,000 dilution, 13901; Cell Signaling Technology), which was used as the internal control. The efficiency of transfection was evaluated by using anti-GFP antibody (1:3,000 dilution, AE011; ABclonal, Wuhan, China). Goat anti-rabbit IgG-HRP (1:5,000 dilution, M21001; Abmart, Shanghai, China) was used as the secondary antibody and incubated with the membrane for 1 h at 25 °C. Protein bands were visualized using the ECL Western Blotting Substrate (Tanon, Shanghai, China).

Proteins from the testes of adult mice were extracted using a homogenizer in RIPA lysis buffer supplemented with a 1% protease inhibitor cocktail. After quantifying the protein concentration, equal amounts of protein were used for western blotting, as described above. Custom-made polyclonal antibody against ADGB (300–425aa, rabbit anti-mouse, 1:1,000 dilution; ABclonal) was used to determine protein expression levels. Alpha-Tubulin (1:1,000 dilution, SAB5600206; Sigma-Aldrich, St. Louis, MO, USA) was used as the loading control.

For co-immunoprecipitation, cells were lysed in NP-40 lysis buffer that was supplemented with a 1% protease inhibitor cocktail. Anti-FLAG affinity gel beads (Bimake) or anti-HA magnetic beads (Bimake) were then added and incubated at 4 °C for 2–3 h. The resulting immunocomplexes were washed 3–4 times with lysis buffer and boiled for 10 min after adding 10 μL 2×SDS-PAGE sample loading buffer. Western-blotting was conducted to evaluate the binding of ADGB to CaM. Afterward, the membrane was incubated at 4 °C with anti-CaM primary antibody (1:3,000 dilution, ab45689; Abcam, Cambridge, MA, USA), anti-FLAG primary antibody, or anti-Vinculin primary antibody which was used as the internal control. Goat anti-rabbit IgG-HRP was used as the secondary antibody.

Generation of knockout mice using CRISPR/Cas9

Adgb-knockout mouse model was generated using CRISPR/Cas9 technology (constructed by Cyagen Biosciences).

In brief, the following three guide RNA (gRNA) targets: gRNA1-CACAGGATGTACATAAGAGTGGG, gRNA2-GTTAAAGAACATCGGAAGAGG, and gRNA3-CGA GCATATATGTAAAAGAGAGG, were chosen to produce a deletion of the *Adgb* exon 2–29. The Cas9 mRNA and gRNAs were pooled and injected into the zygotes of C57BL/6N mice and the injection volumes were listed in Supplementary Table S1. The F0 founder mice were crossed with WT C57BL/6N mice to obtain offspring. Then heterozygotes were intercrossed until homozygous offspring were obtained. The offspring were genotyped via PCR-Sanger sequencing of the mouse genomic DNA and the genotyping primers are also listed in Supplementary Table S1.

Semen parameter analysis

Spermatozoa from the cauda epididymis were released into modified human tubal fluid medium (Millipore, Billerica, MA, USA) at 37 °C in a 5% CO₂ incubator for 45 min. After the swimming of sperm, 30 μL of supernatant was added to the counting chamber (11917C1, Leja, Netherlands). Then the computer-assisted sperm analysis program HTM-TOX-IVOS (Hamilton Thorn Inc, Beverly, MA, USA) was used to analyze sperm motility. Three pairs of 8-week-old *Adgb*^{+/+} and *Adgb*^{−/−} mice were included. The extracted sperm were washed with phosphate-buffered saline (PBS) 2–3 times and stored at –80 °C.

Daily sperm production (DSP) in testis was assessed according to the protocol established by Kyjovska et al. (2013), with modifications. In short, the left testicle was homogenized by ultrasonic processor (JY92-IIN, Alwhals, Shanghai, China) in 1 mL of 0.05% triton X-100 homogenization buffer [0.9% NaCl (10019318) and 0.05% triton X-100 (30188928); Sinopharm Chemical Reagent Co. Ltd, Shanghai, China] for 2 min (40% power, 3 s on, 6 s off). Then put the homogenate on ice for 30 min, a 200-μL aliquot of homogenate was stained with equivalent 0.04% Trypan blue (2067964, Thermo Fisher Scientific, Waltham, MA, USA). Spermatids could be counted in hemocytometer (WG607, Servicebio, Wuhan, China) under light microscope (EVOS M7000 Imaging System, Thermo Fisher Scientific) and DSP was then calculated. The whole left epididymis was separated and processed according to the above procedures, and then the total sperm number was counted.

Histological analysis and periodic acid-schiff staining

Freshly dissected testes and different parts of the epididymis were fixed in animal testicular tissue fixative (G1121-500ML, Servicebio), the main ingredients of which are formaldehyde solution, ethanol, and glacial acetic acid. Then the tissues were embedded in paraffin for histological

analysis. Subsequently, the specimens were cut into 5 µm sections, followed by deparaffinization, benzene removal, hydration, and staining with Periodic acid-Schiff. The procedures for staining are as follows. 0.5% periodic acid that has been freshly prepared was added onto the sections, and the slides were kept out of light for 5 min. After being rinsed with purified water, the Schiff solution was added onto the slides and kept in the dark for 20 min at 25 °C. After washing with purified water, the slides were air-dried and mounted in neutral balsam (10,004,160, Sinopharm). Images were taken with a light microscope.

Apoptosis analysis by TUNEL assay

The TUNEL assay was used to evaluate testicular and epididymal apoptosis using a TMR (red) TUNEL Cell Apoptosis Detection Kit (Servicebio). Briefly, testicular and epididymal paraffin sections were dewaxed, rehydrated, and then incubated with DNase-free Proteinase K for 30 min at 37 °C. Thereafter, tissue sections were incubated with a TUNEL reaction mixture at 37 °C for 1–2 h. Negative controls underwent the same procedure but without the TdT enzyme. After staining the nuclei with 4',6-diamidino-2-phenylindole (DAPI), red-stained apoptotic cells were identified under a fluorescence microscope (ECLIPSE Ci-L, Nikon, Tokyo, Japan).

Scanning and transmission electron microscopy

For scanning electron microscopy, washed sperm from the cauda epididymis were deposited on poly L-lysine-coated coverslips and then fixed in 2.5% phosphate-buffered glutaraldehyde at 4 °C for 2 h. Next, the coverslips were washed thrice for 10 min each in PBS, followed by fixation in 1% OsO₄ at 4 °C for 1 h. Thereafter, the samples were dehydrated using an ascending gradient of 30, 50, 75, 95, and 100% cold ethanol and then dried using a Quorum K850 Critical Point Dryer (Quorum Technologies, Lewes, UK). Finally, the coverslips were attached to specimen holders, and spermatozoa were coated with gold particles before observation using an SU8010 scanning electron microscope (Hitachi, Tokyo, Japan).

For transmission electron microscopy, the samples were first fixed overnight with 2.5% phosphate-buffered glutaraldehyde at 4 °C. After washing with 0.1 M phosphate buffer, samples were re-fixed with 1% OsO₄ at 4 °C for 1–2 h. Next, the samples were dehydrated with an ethanol gradient and embedded in Epon812 following standard procedures. Finally, ultrathin sections were stained with uranyl acetate and lead citrate for observation under a transmission electron microscope (CM-120, Philips, Netherlands).

Intracytoplasmic sperm injection in mice

Female B6D2F1 mice at 6–8 weeks of age were superovulated via intraperitoneal injection of 10 IU pregnant mare serum gonadotropin (Ningbo Second Hormone Factory, Zhejiang, China), followed 48 h later by an injection of 10 IU human chorionic gonadotropin (Ningbo Second Hormone Factory). After a further 14–15 h, cumulus-oocyte complexes were collected from the ampulla, and the cumulus cells were removed using hyaluronidase (100 IU/mL) prepared in M2 medium (Sigma-Aldrich) to obtain MII oocytes. Spermatozoa were subjected to ultrasound to acquire the heads. Subsequently, single sperm heads were injected into the cytoplasm of WT oocytes using a Piezo Micromanipulator (Eppendorf, Hamburg, Germany). After intracytoplasmic sperm injection (ICSI), oocytes were transferred into KSOM medium and incubated at 37 °C with 5% CO₂ to observe fertilization and embryo development.

Screening for proteins that interact with ADGB using mass spectrometry

Testis tissues were homogenized as described above. After quantification, equal amounts of protein were incubated overnight with anti-ADGB antibody at 4 °C on a shaker. Protein A/G magnetic beads—for immunoprecipitation (Bimake)—were then added to the mix and incubated at 4 °C for 2 h. Next, proteins bound to washed beads were eluted in 5×SDS-PAGE sample loading buffer at 95 °C for 10 min and then separated by SDS-PAGE on 10% gels. Subsequently, each gel lane was cut out, finely chopped, and digested with trypsin, and the analysis was performed on an Orbitrap Exploris 480 mass spectrometer (Thermo Fisher Scientific) coupled to an EASY-nLC 1000 nanoflow HPLC (Thermo Fisher Scientific). MS data were searched against the UniProtKB mouse database, and the cutoff of the global false discovery rate for peptide and protein recognition was set at 0.01. To validate the interacting proteins, the following primary antibodies were used: anti-CFAP69 (1:1,000 dilution, A18193; Abclonal), anti-SPEF2 (1:1,000 dilution, BT-AP12744; BT lab, Shanghai, China), and anti-GAPDH (1:1,000 dilution, 5174S; Cell Signaling Technology).

Statistical analysis

All experiments were independently performed at least three times, and GraphPad (GraphPad Software Inc., San Diego, CA, USA) was used for statistical analysis. Two-tailed Student's *t*-test or one-way ANOVA was used to assess statistical differences, and a *P*<0.05 was considered significant.

Results

Clinical features and *ADGB* variant identification

Using whole exome sequencing and bioinformatics analysis, we identified compound heterozygous *ADGB* variants in a patient diagnosed with asthenozoospermia. The sperm motility of the patient was below the lower reference limits recommended in the sixth edition of the World Health Organization laboratory manual (WHO 2021) (Table 1).

Proband II-1 carried the *ADGB* variants c.1277delT (p.Leu426CysfsTer9) and c.3319G>T (p.Glu1107Ter), with

c.1277delT—resulting in a frameshift and a subsequently truncated protein—and c.3319G>T—producing a new stop codon causing the protein to terminate prematurely—thus suggesting their strong deleterious effects (Fig. 1a). The amino acids altered by the two variants are highly conserved among different species (Fig. 1b). During the in vitro fertilization (IVF) procedure, the patient's sperm could not fertilize the oocytes, even though the number of oocytes retrieved and their maturity were normal. Following ICSI, six oocytes were collected, of which three were fertilized, and these developed into embryos and were frozen for transplantation (Table 2).

All variants were validated by Sanger sequencing. However, these variants were not found in the gnomAD or ExAC databases or our in-house control database (which includes more than 1,000 couples with normal fertility),

Table 1 The semen parameters of the individual carrying variants of *ADGB*

Semen analysis	II-1	Low reference limits according to the WHO criteria
Age	33	/
Semen volume (mL)	2.7	1.4 (1.3–1.5)
Sperm concentration ($10^6/\text{mL}$)	90.4	16 (15–18)
Total sperm (10^6)	244.1	39 (35–40)
Progressive motility (%)	2.4*	30 (29–31)
Total motility	12.5*	42 (40–43)
(Progressive + Non-progressive, %)		

*Value is lower than the reference limits

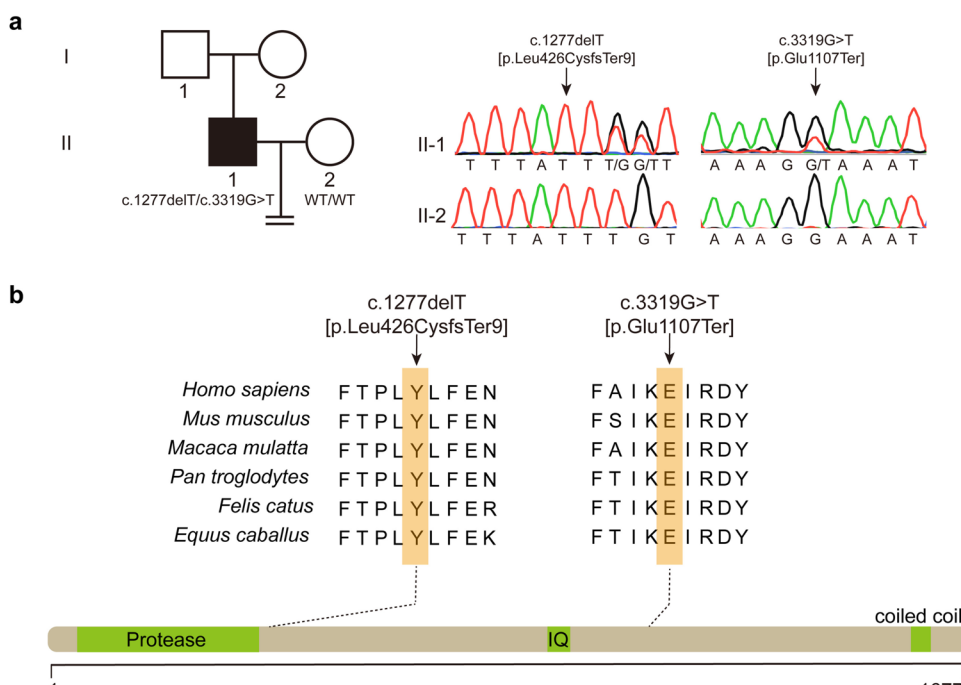
Table 2 The IVF/ICSI history of the affected individual in this study

Assisted reproductive treatment and developmental outcomes	II-1	
	IVF	ICSI
Cycles	1	2
No. of oocytes retrieved	9	6
No. of mature oocytes (MII)	7	6
No. of fertilized oocytes (2PN)	0	3
No. of good-quality embryos	0	3

Good quality embryo: Grade 1, ≥ 7 –8 cells

ICSI (intracytoplasmic sperm injection), IVF (in vitro fertilization)

Fig. 1 Identification of compound heterozygous variants of *ADGB* in an infertile male with asthenozoospermia. **a** Pedigree of the family with *ADGB* variants. The open and filled signs represent the unaffected and affected individuals, respectively. Validation by Sanger sequencing is shown. **b** Locations and conservation analysis of the variants in the proband. The positions of variants are labeled in the protein structures of *ADGB*, and conserved amino acids are indicated by the alignment of six species



suggesting their rarity. Therefore, we speculated that these *ADGB* variants were responsible for the patient's fertility defects.

***ADGB* variants impair the binding of *ADGB* to CaM**

To assess the impact of the variants on *ADGB* activity, we first measured WT and mutant protein expression in HEK 293T cells. p.Leu426CysfsTer9 and p.Glu1107Ter resulted in truncated proteins. In addition, p.Glu1107Ter produced significantly decreased protein levels (Fig. S1a and S1b). It has been reported that *ADGB* possesses a CaM-binding IQ motif (Hoogewijs et al. 2012); therefore, we analyzed the effect of the variants on the binding of *ADGB* to CaM. Co-immunoprecipitation showed that the WT and p.Glu1107Ter mutant could interact with CaM but not the p.Leu426CysfsTer9 mutant (Fig. S1c), suggesting that this mutant could cause functional impairment of *ADGB*. Unfortunately, HA-tagged CaM failed to pull down FLAG-tagged *ADGB* in the co-expressed system (Fig. S1d), which could be due to the protein binding properties or experimental conditions.

***Adgb*^{-/-} male mice are infertile due to sperm deformity and loss of motility**

To study the pathogenesis of *ADGB* variants, we generated *Adgb* knockout mice using CRISPR/Cas9 technology (Fig. S2 and Table S1). The *ADGB* protein was completely absent in the testes of *Adgb*^{-/-} mice (Fig. 2a). When both male and female *Adgb*^{-/-} mice were mated with WT mice, the *Adgb*^{-/-} males were infertile (Fig. 2b). The testes size of *Adgb*^{-/-} male mice were decreased, and the ductus within the cauda epididymis was more transparent compared with that of *Adgb*^{+/+} male mice (Fig. 2c), suggesting less sperm was presented.

To determine the cause of infertility in *Adgb*^{-/-} male mice, we examined the physiological parameters of the sperm in the cauda epididymis by computer-assisted sperm analysis. The sperm concentration of *Adgb*^{-/-} mice was significantly lower than that in *Adgb*^{+/+} mice (Fig. 2d). *Adgb*^{+/+} sperm had normal motility and normal distribution of different motive classifications, but the sperm were completely immobile in *Adgb*^{-/-} mice (Fig. 2d). We next examined the morphology of epididymal sperm by light microscopy. Sperm from the *Adgb*^{+/+} male mice had well-developed, hook-shaped heads and long smooth tails. In contrast, sperm from *Adgb*^{-/-} male mice had malformed heads and tails and contained a large amount of cytoplasmic material, residual bodies, and sloughed germ cells (Fig. S3).

Spermatogenesis is disrupted in *Adgb*^{-/-} male mice

Sperm are produced in the seminiferous tubules of the testis and then released into the epididymis. To determine the reasons for the observed reduction in sperm output and terato-spermia in *Adgb*^{-/-} mice, we first visualized the morphology of the testis and epididymis using histochemical staining. There were only a few deformed spermatids in the seminiferous epithelia in *Adgb*^{-/-} mice, and almost none were released into the lumen, showing a spermiation failure (Fig. 3a). Consistent with the expression pattern of *Adgb* during the different stages of spermatogenesis in which round spermatids differentiate into elongating spermatids and form the flagellum (Keppner et al. 2022), no regular flagella were observed in *Adgb*^{-/-} spermatids and there was no mature sperm.

The spermatogenesis process in the testicles of mice is divided into 12 stages, which could be observed in both *Adgb*^{+/+} and *Adgb*^{-/-} mice (Fig. 3b). Although the arrangement of spermatogonia and spermatocytes and meiotic events (stages X–XII) appeared normal in *Adgb*^{-/-} mice, spermatid deformation and abnormal maturation were observed in the seminiferous epithelia. Notably, testicular sections of *Adgb*^{-/-} male mice exhibited more round spermatids, but elongating or elongated spermatids were fewer than those in *Adgb*^{+/+} males (Fig. 3c). These spermatids were barely released from the Sertoli cells due to poor quality. To further explain the reasons for limited count of sperm in *Adgb*^{-/-} mice, we assessed the DSP in testes and total epididymal sperm counts. We could show that *Adgb*^{-/-} male mice have a significant reduction in DSP and epididymal sperm counts when compared with WT ones (Fig. S4). It suggested that even elongating or elongated spermatids were generated in *Adgb*^{-/-} male mice, but the number was significantly lower. The spermatids could not move to the lumen and enter the epididymis to undergo further maturation due to defects in cell metamorphosis. This is likely the reason for the reduced number of epididymal sperm in *Adgb*^{-/-} mice.

Testicular spermatids from *Adgb*^{-/-} mice could fertilize oocytes by ICSI

We used scanning electron microscopy to further analyze the morphological defects in sperm. Similar to what was observed under a light microscope, sperm from *Adgb*^{+/+} mice presented with long smooth tails and normally condensed heads. However, multiple abnormalities were observed in the sperm of *Adgb*^{-/-} mice, including more oblong, axe-shaped, and irregularly shaped heads, as well as anomalously shaped tails, including bobtails, curly tails, swollen mid-sections, and fine tails (Fig. 4a).

We further observed the ultrastructure of sperm from the cauda epididymis using transmission electron microscopy. The structural features further revealed misshapen heads,

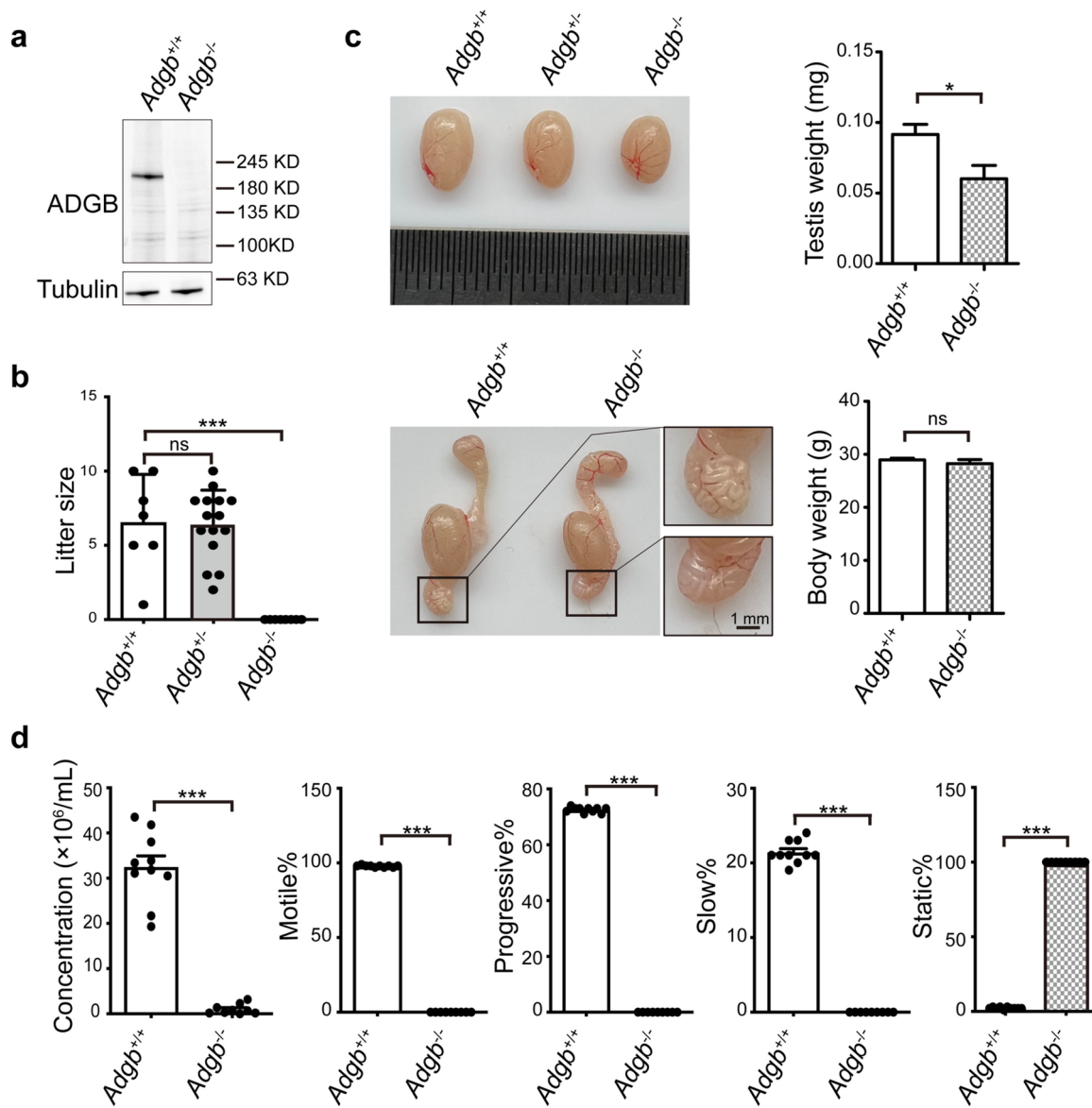


Fig. 2 Homozygous knockout of *Adgb* leads to male infertility in the mouse model. **a** The ADGB protein was completely absent in the testes of *Adgb*^{-/-} male mice. Tubulin was used as the loading control. **b** WT, heterozygous, and homozygous knockout males were mated with WT females separately, and the *Adgb*^{-/-} male mice were unable to produce offspring. Data are shown as the means \pm SEM ($n=7$, *** $p<0.0001$, ns, not significant). **c** The testis size of *Adgb*^{-/-} male

mice were reduced when compared with that of WT, and the cauda epididymis was also notably smaller ($n=5$, * $p<0.05$). **d** Sperm concentration, motility, and progressive motility were determined by computer-assisted sperm analysis and were significantly lower in *Adgb*^{-/-} mice. The proportion of immobile sperm increased significantly in *Adgb*^{-/-} mice. Data are shown as means \pm SEM ($n=3$, *** $p<0.0001$)

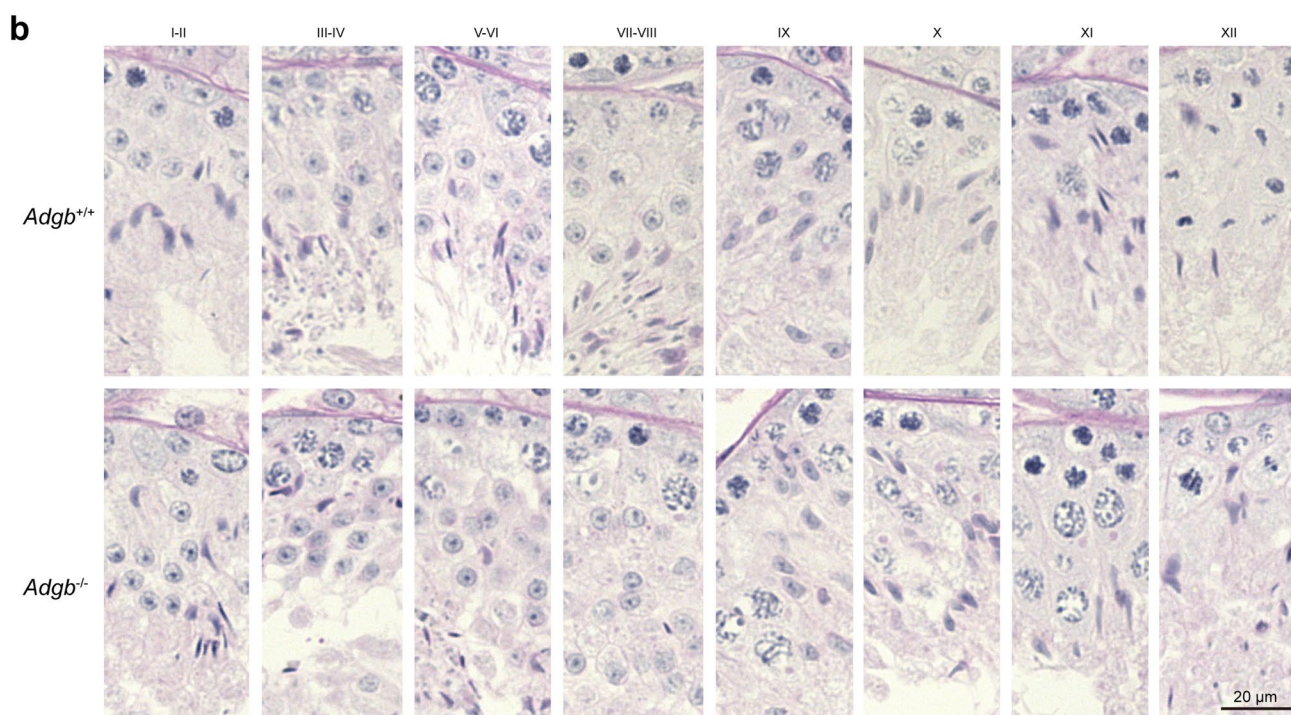
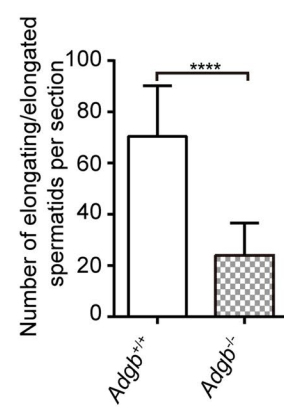
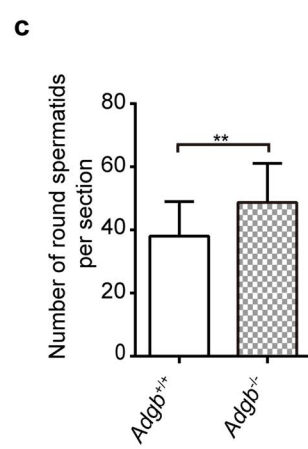
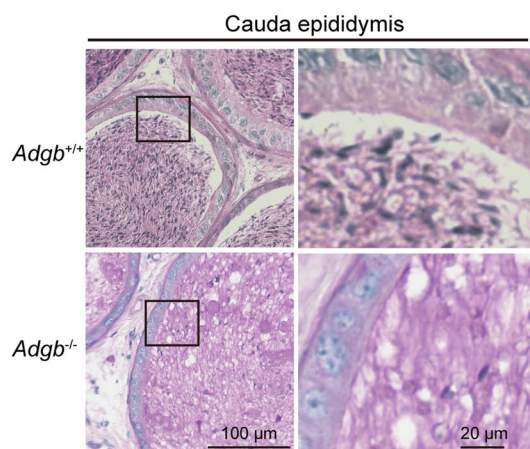
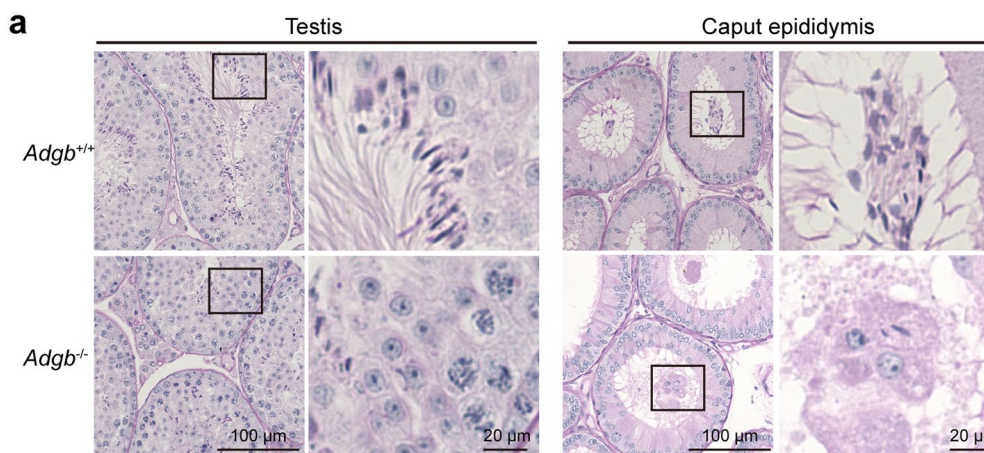
incomplete acrosomes, deficient neck joints, disorganized axonemes that failed to line up around the flagella, defective “9+2” structures, misaligned microtubules, and mitochondrial disorders in the formation of the midpieces of elongated spermatids in *Adgb*^{-/-} mice (Fig. 4b).

Because of the severe deformities and lack of motility, WT oocytes could not be fertilized by *Adgb*^{-/-} sperm through IVF. Therefore, we attempted ICSI to rescue the infertility of *Adgb*^{-/-} mice. The results indicated that sperm from cauda

epididymis could not fertilize oocytes effectively, whereas spermatids isolated from testes could, eventually, resulting in blastocyst development (Fig. S5 and Table S2).

Adgb deletion induces apoptosis in the epididymis

To study the cause of limited elongated spermatid release, we assessed the state of spermatogenic cells in *Adgb*^{+/+} and *Adgb*^{-/-} mice. TUNEL staining of *Adgb*^{-/-} male



◀Fig. 3 Histological images of the testis and epididymis structures of *Adgb^{+/+}* and *Adgb^{-/-}* mice stained with Periodic acid-Schiff. **a** Testicular and epididymis sections stained with Periodic acid-Schiff. The detail of the area enclosed by the square is shown on the right side of the original image with 4.5× magnification. The number of sperm in the lumen was decreased in *Adgb^{-/-}* mice compared with that in *Adgb^{+/+}* mice. **b** All stages of the seminiferous epithelial cycle are labeled with Roman numerals above the images. Intact spermatogenic lumen and neatly arranged spermatogenic cells were present, but there were few elongating and elongated spermatids in *Adgb^{-/-}* mice with spermiation failure. **c** Quantification of round, elongating or elongated spermatids in the maximum cross section of testes from *Adgb^{+/+}* and *Adgb^{-/-}* mice. ***p*<0.01, ****p*<0.0001

mice testes sections showed that there were unreleased apoptotic spermatids in the spermatogenic epithelium, but there was no significant difference between *Adgb^{+/+}* and *Adgb^{-/-}* mice (Fig. 5a and Fig. S6a). The results in the caput epididymis were consistent with this observation (Fig. 5b and Fig. S6b). In the cauda epididymis, the number of apoptotic cells per tubule was significantly increased in *Adgb^{-/-}* mice (Fig. 5c and Fig. S6c). The high rate of apoptotic events might further aggravate the decrease of sperm.

ADGB deficiency might affect assembly of sperm structure by influencing CFAP69 or SPEF2

To further analyze the molecular events affected by the loss of ADGB, we performed MS on testis proteins from *Adgb^{+/+}* and *Adgb^{-/-}* male mice. Only proteins enriched in the WT have been selected, by screening the quality of peptides and the abundance of expression, we identified 42 candidates that specifically bound to WT ADGB (Table S3). Functional analysis based on Gene Ontology term enrichment by using the R package clusterProfiler (Yu et al. 2012; Wu et al. 2021) confirmed that most of these genes were related to sperm motility, sperm structural assembly, spermatid development and differentiation, and regulation of apoptosis (Fig. 5d). These results were in line with the observed structural and functional defects in the sperm from *Adgb^{-/-}* male mice. Furthermore, we selected CFAP69 and SPEF2, which were known to play a key role in affecting the structure of sperm flagella to verify the MS data. Immunoprecipitation on testis protein lysates showed that ADGB could indeed bind to CFAP69 or SPEF2, and this binding was absent in *Adgb^{-/-}* male mice (Fig. 5e and Fig. S7). These results suggested that ADGB plays an important role in the structural assembly of sperm, but more evidence is still needed to demonstrate the specific mechanism. Besides, we assessed the binding of ADGB to CaM, unlike the results in cells, ADGB was unable to pull down CaM in testes (Fig. S8).

Discussion

Asthenozoospermia is a common cause of male infertility, and some disease-causing genes, including those associated with structural proteins required for the proper formation of the sperm flagellum and proteins involved in energy metabolism, have been reported (Shahrokhi et al. 2020). In addition, non-coding and circular RNAs have also been shown to be involved in asthenozoospermia (Manfreola et al. 2020). However, despite all of these studies, the etiology of asthenozoospermia remains to be fully elucidated.

In this study, we identified compound heterozygous *ADGB* variants through whole exome sequencing in a patient with male infertility caused by asthenozoospermia. In addition, we generated an *Adgb* knockout mouse model and found that *Adgb^{-/-}* male mice were infertile, phenotype of which were similar to Keppner et al. (2022). These data show that *ADGB* has certain correlations with male fertility. Further detection of variants in more patients will help elucidate the function of *ADGB*.

IQ motif-containing proteins that are known to bind to CaM have a wide diversity of biological functions (Bahler and Rhoads 2002). In addition, the IQ motif-containing genes *IQCD* (Zhang et al. 2019a, b), *IQCF1* (Fang et al. 2015), and *IQCG* (Harris et al. 2014) have been shown to affect sperm structure and function. The p.Leu426CysfsTer9 mutant cannot bind to CaM, which may result in obstruction of the calcium signaling pathway and subsequent fertilization failure. As for the function of the globin domain and protease domain, more studies are needed. We also tested the binding of ADGB to CaM in mouse testes, but the full-length ADGB protein was found not to bind CaM, which would explain why CaM is not present in the MS data. In the study of Keppner et al. (2022), they suggested that a truncated protein covering the globin and IQ domains could display ADGB-CaM interaction. Therefore, we speculated that the inability of human CaM to pull down ADGB in the overexpression system may be due to the limited ability of CaM to recognize ADGB. It is also possible that the interaction is dependent on calcium ions or other experimental conditions.

We demonstrated that spermatogenesis in *Adgb^{-/-}* mice was abnormal, especially in spermiogenesis. Scanning and transmission electron microscopy showed severe malformations of the head and tail during spermatogenesis in *Adgb^{-/-}* mice, and spermatids that were unable to complete spermiogenesis were trapped in the spermatogenic epithelium. Some of the spermatozoa that were transported to the epididymis eventually underwent apoptosis, which exacerbated the decline in sperm count. Semen analysis showed

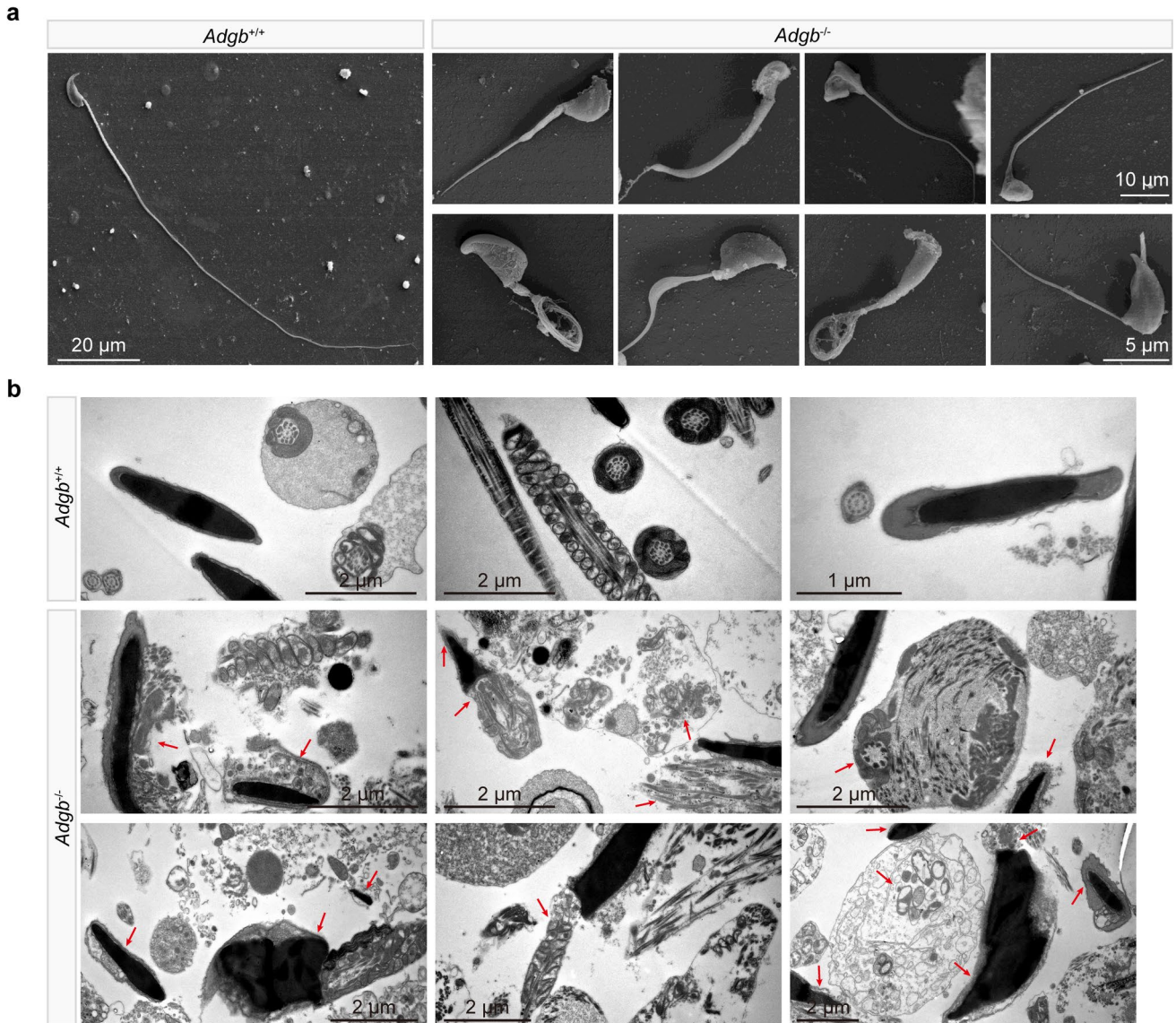


Fig. 4 Ultrastructural assessment of sperm in *Adgb^{-/-}* mice. **a** Scanning electron microscope images of sperm ultrastructure showing severe malformations in the sperm heads and tails of *Adgb^{-/-}* mice. **b** Transmission electron microscopy images of the sperm ultrastruc-

ture. The red arrows indicate the defects in the sperm from *Adgb^{-/-}* mice, including incomplete acrosomes, atypical nuclei, irregular neck regions, disordered mitochondrial sheaths, and the absence of "9+2" microtubules

that the decrease in sperm motility was consistent in the patient with *ADGB* variants and *Adgb^{-/-}* male mice. Sperm from *Adgb^{-/-}* male mice were unable to fertilize oocytes via IVF due to severe malformation and lack of motility, but the spermatids separated from testes could fertilize oocytes through ICSI followed by blastocyst development. ICSI with testicular spermatozoa is mainly used to treat non-obstructive azoospermia or oligozoospermia. Besides, successful birth could be attained after ICSI with testicular immotile spermatozoa from patient with total MMAF (Zhang et al. 2021), which suggests that testicular spermatozoa can exert fertilization potential in the absence

of normal mature sperm. Sperm DNA fragmentation or abnormal chromatin will decline the fertility of mouse sperm. Studies have shown that testicular spermatozoa possess less genome damage due to its lower exposure to reactive oxygen species than sperm storing and transporting along the epididymis (Zhang et al. 2019a, b; Arafa et al. 2018; Suganuma et al. 2005). During the process of maturation of spermatozoa in the epididymis, there will be some modifications, such as the changes in membrane lipid composition and the form of flagellar movement. In this study, the proportion of apoptosis in the epididymis increased significantly in *Adgb^{-/-}* male mice. These may

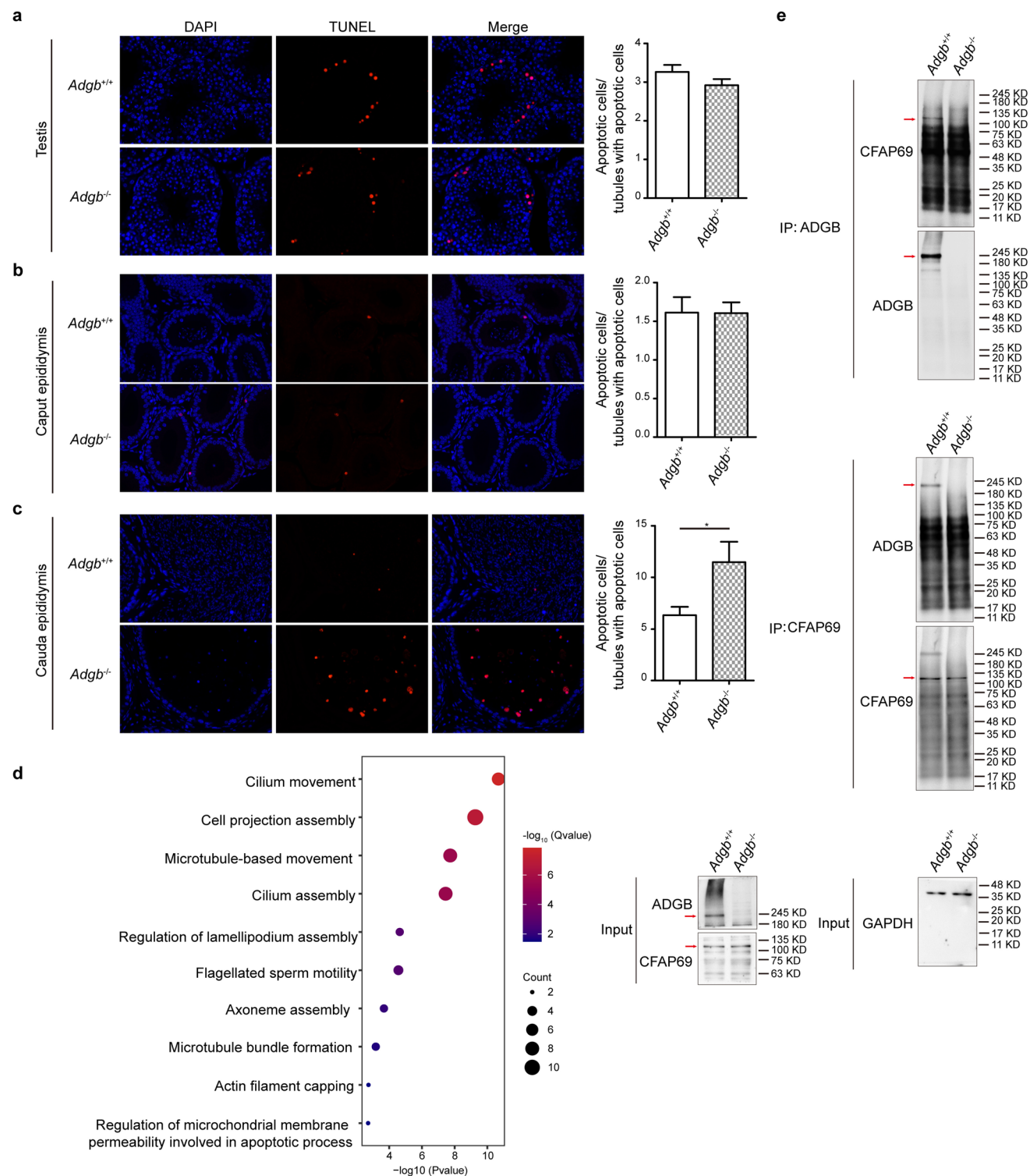


Fig. 5 Apoptotic signals in the testis and epididymis and identification of ADGB binding proteins. Terminal deoxynucleotidyl transferase nick-end-labeling (TUNEL) staining revealed that apoptotic cells in the testis (**a**) and the caput epididymis (**b**) were not significantly different between *Adgb*^{+/+} and *Adgb*^{-/-} mice. **c** The number of apoptotic cells in the cauda epididymis of *Adgb*^{-/-} mice was significantly increased ($n=3$, $*p<0.05$). **d** A total of 42 molecules that specifically bind to ADGB were identified through mass spectrometry, and these were analyzed according to Gene Ontology annotations. **e** The interaction between ADGB and CFAP69 in the testis was verified by co-immunoprecipitation. The red arrows indicate the target bands

cantly increased ($n=3$, $*p<0.05$). **d** A total of 42 molecules that specifically bind to ADGB were identified through mass spectrometry, and these were analyzed according to Gene Ontology annotations. **e** The interaction between ADGB and CFAP69 in the testis was verified by co-immunoprecipitation. The red arrows indicate the target bands

explain why epididymal sperm have a weaker fertilization potential than testicular spermatids. There were phenotypic differences between mice and humans. First of all, ADGB was completely deleted in mice, resulting in greater functional impact, and the sperm not only had lower motility but were also more severely deformed. In contrast, in vitro, *ADGB* variants leading to protein truncation rather than complete absence might retain some functions, especially the p.Glu1107Ter mutant, which could still bind to CaM. Secondly, full-length human ADGB could bind to CaM while full-length mouse ADGB could not. And lastly, it is possible that there were considerable differences in the molecular mechanism of ADGB affecting male fertility between humans and mice.

Mass spectroscopy showed that ADGB might interact with multiple proteins and signaling pathways, thereby affecting spermatogenesis. These included the flagella-related genes *Spef2* (Li et al. 2021) and *Cfap69* (He et al. 2019), the motility-related genes *Tekt5* (Cao et al. 2011), *Tekt4* (Roy et al. 2007), and *Tekt3* (Roy et al. 2009), the manchette-related genes *Lrguk* (Okuda et al. 2017) and *Smrp1* (Matsuoka et al. 2008), and the sperm capacitation gene *Ropn1l* (Zhang et al. 2016). Protein levels of cofilin-1 (CFI1) was increased in *Pfn3*^{-/-} testes, loss of which impairs spermiogenesis by affecting acrosome biogenesis, autophagy, manchette development and mitochondrial organization (Umer et al. 2021). Proteomic analysis revealed CFI1 as a candidate protein that affect the quality of spermatozoa from boars on plateaus (Zhao et al. 2021). Apoptosis-related genes *Hnrnpk* (Chen et al. 2021) and *Slc25a5* (Li et al. 2019) were also included. The interaction of ADGB with CFAP69 or SPEF2 has been verified by co-immunoprecipitation, further strengthening the evidence that ADGB deficiency may affect sperm morphology. “Club-shaped” elongating spermatids in stages X–XII could be observed in the sections of *Adgb*^{-/-} testes; these seemed to be caused by failure to disassemble the manchette, which is also one of the reasons for sperm motility deficiency. Therefore, it is speculated that ADGB might disturb manchette formation. The identification of these interacting proteins hinted the important role of ADGB in male reproduction.

Although a recently published study reported an infertility phenotype and abnormal spermatogenesis in ADGB-deficient male mice (Keppner et al. 2022), our present study shows several different findings. In our study, we have shown that *ADGB* variants may contribute to male infertility. Although ADGB-deficient male mice showed abnormal sperm head shaping and flagellum formation, proband's sperm had no obvious structural defects. And the published study declared that full-length mouse ADGB did not interact with CaM. In contrast, we demonstrated that intact human ADGB could bind to CaM in cell-based overexpression systems. This varying binding characteristics might also partially explain the phenotypic

differences between humans and mice. In addition, blastulas could be obtained after ICSI with *Adgb*^{-/-} sperm, which suggesting a potential treatment strategy for those patients with variants of *ADGB*.

In summary, we identified *ADGB* variants in a patient with asthenozoospermia. In vitro functional experiments and analysis of the knockout mouse model proved that ADGB probably plays an important role in male fertility and spermatogenesis. These results further expand the genetic causes of male infertility due to asthenozoospermia and provide a theoretical basis for using *ADGB* as a potential genetic diagnostic marker for infertile males suffering from recurrent IVF or ICSI failure.

Supplementary Information The online version contains supplementary material available at <https://doi.org/10.1007/s00439-023-02546-0>.

Acknowledgements We are deeply grateful to all the patients and their families for the participation. We would like to thank Mrs. Hong Gao from the electron microscope platform of the School of Basic Medical Sciences of Fudan University and the MS platform of the Institutes of Biomedical Sciences of Fudan University.

Author contributions ZY and LW collected the samples. RQ performed the experiments. BC and QL analyzed the data. RQ and QS wrote the paper. XS, YK, LW, and QS conceived and designed the experiments. JM, LZ, and WW treated the mice. ZZ, RL, and YZ constructed the plasmids and prepared the electron microscope samples. JD and QL took and processed the images. All authors approved the final manuscript.

Funding This work was sponsored by the National Natural Science Foundation of China (82201767), the Shanghai Sailing Program (21YF1418300), and the SHIPM-PI fund No. JY201801 from Shanghai Institute of Precision Medicine, Ninth People's Hospital Shanghai Jiao Tong University School of Medicine.

Data availability The data underlying this article are available in the article and in its online supplementary material.

Declarations

Conflict of interest None of the authors declare any conflict of interest.

Ethical approval All experiments were approved by the Ethics Committee of the Medical College of Fudan University and the Ninth Hospital affiliated with Shanghai Jiao Tong University. The study was performed conforming to the current Declaration of Helsinki and all individuals provided written informed consent. The animal experimental operation was approved by the ethics committee (2022JS-029).

Consent to participate All contributors provided written informed consent to participate in this study.

Consent to publish All contributors provided written informed consent for publication.

References

- Agarwal A, Mulgund A, Hamada A, Chyatte MR (2015) A unique view on male infertility around the globe. *Reprod Biol Endocrinol* 13:1–9. <https://doi.org/10.1186/s12958-015-0032-1>
- Akbari A, Pipitone GB, Anvar Z, Jaafarinia M, Ferrari M, Carrera P, Totonchi M (2019) ADCY10 frameshift variant leading to severe recessive asthenozoospermia and segregating with absorptive hypercalciuria. *Hum Reprod* 34:1155–1164. <https://doi.org/10.1093/humrep/dez048>
- Arafa M, AlMalki A, AlBadr M, Burjaq H, Majzoub A, AlSaid S, Elbadisi H (2018) ICSI outcome in patients with high DNA fragmentation: Testicular versus ejaculated spermatozoa. *Andrologia* 50. <https://doi.org/10.1111/and.12835>
- Bahler M, Rhoads A (2002) Calmodulin signaling via the IQ motif. *Febs Lett* 513:107–113. [https://doi.org/10.1016/s0014-5793\(01\)03239-2](https://doi.org/10.1016/s0014-5793(01)03239-2)
- Ben KM, Coutton C, Zouari R, Karaouzene T, Rendu J, Bidart M, Yassine S, Pierre V, Delaroche J, Hennebicq S, Grunwald D, Escalier D, Pernet-Gallay K, Jouk PS, Thierry-Mieg N, Toure A, Arnoult C, Ray PF (2014) Mutations in DNAH1, which encodes an inner arm heavy chain dynein, lead to male infertility from multiple morphological abnormalities of the sperm flagella. *Am J Hum Genet* 94:95–104. <https://doi.org/10.1016/j.ajhg.2013.11.017>
- Cao W, Ijiri TW, Huang AP, Gerton GL (2011) Characterization of a novel tektin member, TEKT5, in mouse sperm. *J Androl* 32:55–69. <https://doi.org/10.2164/jandrol.109.009456>
- Chen CC, Yang JH, Fu SL, Lin WJ, Lin CH (2021) Arginine Methylation of hnRNP K Inhibits the DDX3-hnRNP K Interaction to Play an Anti-Apoptosis Role in Osteosarcoma Cells. *Int J Mol Sci.* <https://doi.org/10.3390/ijms22189764>
- Fang P, Xu W, Li D, Zhao X, Dai J, Wang Z, Yan X, Qin M, Zhang Y, Xu C, Wang L, Qiao Z (2015) A novel acrosomal protein, IQCF1, involved in sperm capacitation and the acrosome reaction. *Andrology* 3:332–344. <https://doi.org/10.1111/andr.296>
- Gao Y, Wu H, Xu Y, Shen Q, Xu C, Geng H, Lv M, Tan Q, Li K, Tang D, Song B, Zhou P, Wei Z, He X, Cao Y (2021) Novel biallelic mutations in SLC26A8 cause severe asthenozoospermia in humans owing to midpiece defects: Insights into a putative dominant genetic disease. *Hum Mutat* 43:434–443. <https://doi.org/10.1002/humu.24322>
- Hagiuda J, Takasaki N, Oya M, Ishikawa H, Narimatsu H (2020) Mutation of GALNTL5 gene identified in patients diagnosed with asthenozoospermia. *Hum Fertil (Camb)* 23:226–233. <https://doi.org/10.1080/14647273.2018.1562239>
- Harris TP, Schimenti KJ, Munroe RJ, Schimenti JC, (2014) IQ motif-containing G (Iqcg) is required for mouse spermiogenesis. *G3 (Bethesda)* <https://doi.org/10.1534/g3.113.009563>
- He X, Li W, Wu H, Lv M, Liu W, Liu C, Zhu F, Li C, Fang Y, Yang C, Cheng H, Zhang J, Tan J, Chen T, Tang D, Song B, Wang X, Zha X, Wang H, Wei Z, Yang S, Saiyin H, Zhou P, Jin L, Wang J, Zhang Z, Zhang F, Cao Y (2019) Novel homozygous CFAP69 mutations in humans and mice cause severe asthenotatospermia with multiple morphological abnormalities of the sperm flagella. *J Med Genet* 56:96–103. <https://doi.org/10.1136/jmedgenet-2018-105486>
- Hoogewijs D, Ebner B, Germani F, Hoffmann FG, Fabrizius A, Moens L, Burmester T, Dewilde S, Storz JF, Vinogradov SN, Hankeln T (2012) Androglobin: A chimeric globin in metazoans that is preferentially expressed in Mammalian testes. *Mol Biol Evol* 29:1105–1114. <https://doi.org/10.1093/molbev/msr246>
- Houston BJ, Riera-Escamilla A, Wyrwoll MJ, Salas-Huetos A, Xavier MJ, Nagirnaja L, Friedrich C, Conrad DF, Aston KI, Krausz C, Tuttelmann F, O'Bryan MK, Veltman JA, Oud MS (2021) A systematic review of the validated monogenic causes of human male infertility: 2020 update and a discussion of emerging gene-disease relationships. *Hum Reprod Update* 28:15–29. <https://doi.org/10.1093/humupd/dmab030>
- Huang B, Lu YS, Li X, Zhu ZC, Li K, Liu JW, Zheng J, Hu ZL (2014) Androglobin knockdown inhibits growth of glioma cell lines. *Int J Clin Exp Pathol* 7:2179–2184
- Joachimiak E, Osinka A, Farahat H, Swiderska B, Sitkiewicz E, Poprzeczk M, Fabczak H, Wloda D (2021) Composition and function of the C1b/C1f region in the ciliary central apparatus. *Sci Rep* 11:11760. <https://doi.org/10.1038/s41598-021-90996-9>
- Keppner A, Correia M, Santambrogio S, Koay TW, Maric D, Osterhof C, Winter DV, Clerc A, Stumpe M, Chalmel F, Dewilde S, Odermatt A, Kressler D, Hankeln T, Wenger RH, Hoogewijs D (2022) Androglobin, a chimeric mammalian globin, is required for male fertility. *Elife*. <https://doi.org/10.7554/elife.72374>
- Koay TW, Osterhof C, Orlando I, Keppner A, Andre D, Yousefian S, Suarez AM, Correia M, Markworth R, Schodel J, Hankeln T, Hoogewijs D (2021) Androglobin gene expression patterns and FOXJ1-dependent regulation indicate its functional association with ciliogenesis. *J Biol Chem*. <https://doi.org/10.1016/j.jbc.2021.100291>
- Kyjovska ZO, Boisen AM, Jackson P, Wallin H, Vogel U, Hougaard KS (2013) Daily sperm production: application in studies of prenatal exposure to nanoparticles in mice. *Reprod Toxicol* 36:88–97. <https://doi.org/10.1016/j.reprotox.2012.12.005>
- Leaver RB (2016) Male infertility: an overview of causes and treatment options. *Br J Nurs* 25: S35–S40. <https://doi.org/10.12968/bjon.2016.25.18.S35>
- Li X, Yan X, Wang F, Yang Q, Luo X, Kong J, Ju S (2019) Down-regulated lncRNA SLC25A5-AS1 facilitates cell growth and inhibits apoptosis via miR-19a-3p/PTEN/PI3K/AKT signalling pathway in gastric cancer. *J Cell Mol Med* 23:2920–2932. <https://doi.org/10.1111/jcmm.14200>
- Li DY, Yang XX, Tu CF, Wang WL, Meng LL, Lu GX, Tan YQ, Zhang QJ, Du J (2021) Sperm flagellar 2 (SPEF2) is essential for sperm flagellar assembly in humans. *Asian J Androl* 24:359. <https://doi.org/10.4103/aja202154>
- Liu C, Miyata H, Gao Y, Sha Y, Tang S, Xu Z, Whitfield M, Patrat C, Wu H, Dulouis E, Tian S, Shimada K, Cong J, Noda T, Li H, Morohoshi A, Cazin C, Kherraf ZE, Arnoult C, Jin L, He X, Ray PF, Cao Y, Toure A, Zhang F, Ikawa M (2020) Bi-allelic DNAH8 Variants Lead to Multiple Morphological Abnormalities of the Sperm Flagella and Primary Male Infertility. *Am J Hum Genet* 107:330–341. <https://doi.org/10.1016/j.ajhg.2020.06.004>
- Lores P, Coutton C, El KE, Stouvenel L, Givelet M, Thomas L, Rode B, Schmitt A, Louis B, Sakheli Z, Chaudhry M, Fernandez-Gonzales A, Mitsialis A, Dacheux D, Wolf JP, Papon JF, Gacon G, Escudier E, Arnoult C, Bonhivers M, Savinov SN, Amselem S, Ray PF, Dulouis E, Toure A (2018) Homozygous missense mutation L673P in adenylate kinase 7 (AK7) leads to primary male infertility and multiple morphological anomalies of the flagella but not to primary ciliary dyskinesia. *Hum Mol Genet* 27:1196–1211. <https://doi.org/10.1093/hmg/ddy034>
- Lu C, Yang D, Lei C, Wang R, Guo T, Luo H (2021) Identification of two novel DNAAF2 variants in two consanguineous families with primary ciliary Dyskinesia. *Pharmacogenomics Pers Med* 14:1415–1423. <https://doi.org/10.2147/PGPM.S338981>
- Manfreola F, Chioccarelli T, Cobellis G, Fasanò S, Ferraro B, Sellitto C, Marella G, Pierantoni R, Chianese R (2020) CircRNA role and circRNA-dependent network (ceRNAs) in asthenozoospermia. *Front Endocrinol (lausanne)* 11:395. <https://doi.org/10.3389/fendo.2020.00395>
- Matsuoka Y, Miyagawa Y, Tokuhiro K, Kitamura K, Iguchi N, Maekawa M, Takahashi T, Tsujimura A, Matsumiya K, Okuyama A, Nishimune Y, Tanaka H (2008) Isolation and characterization

- of the spermatid-specific Smrp1 gene encoding a novel manchette protein. *Mol Reprod Dev* 75:967–975. <https://doi.org/10.1002/mrd.20835>
- Miki K, Willis WD, Brown PR, Goulding EH, Fulcher KD, Eddy EM (2002) Targeted disruption of the Akap4 gene causes defects in sperm flagellum and motility. *Dev Biol* 248:331–342. <https://doi.org/10.1006/dbio.2002.0728>
- Okuda H, DeBoer K, O'Connor AE, Merriner DJ, Jamsai D, O'Bryan MK (2017) LRGUK1 is part of a multiprotein complex required for manchette function and male fertility. *Faseb J* 31:1141–1152. <https://doi.org/10.1096/fj.201600909R>
- Platts AE, Dix DJ, Chemes HE, Thompson KE, Goodrich R, Rockett JC, Rawe VY, Quintana S, Diamond MP, Strader LF, Krawetz SA (2007) Success and failure in human spermatogenesis as revealed by teratozoospermic RNAs. *Hum Mol Genet* 16:763–773. <https://doi.org/10.1093/hmg/ddm012>
- Roy A, Lin YN, Agno JE, DeMayo FJ, Matzuk MM (2007) Absence of tektin 4 causes asthenozoospermia and subfertility in male mice. *Faseb J* 21:1013–1025. <https://doi.org/10.1096/fj.06-7035com>
- Roy A, Lin YN, Agno JE, DeMayo FJ, Matzuk MM (2009) Tektin 3 is required for progressive sperm motility in mice. *Mol Reprod Dev* 76:453–459. <https://doi.org/10.1002/mrd.20957>
- Shahrokh SZ, Salehi P, Alyasin A, Taghiyar S, Deemeh MR (2020) Asthenozoospermia: cellular and molecular contributing factors and treatment strategies. *Andrologia*. <https://doi.org/10.1111/and.13463>
- Suganuma R, Yanagimachi R, Meistrich ML (2005) Decline in fertility of mouse sperm with abnormal chromatin during epididymal passage as revealed by ICSI. *Hum Reprod* 20:3101–3108. <https://doi.org/10.1093/humrep/dei169>
- Sun XH, Zhu YY, Wang L, Liu HL, Ling Y, Li ZL, Sun LB (2017) The catper channel and its roles in male fertility: a systematic review. *Reprod Biol Endocrinol* 15:1–12. <https://doi.org/10.1186/s12958-017-0281-2>
- Toure A, Martinez G, Kherraf ZE, Cazin C, Beurois J, Arnoult C, Ray PF, Coutton C (2021) The genetic architecture of morphological abnormalities of the sperm tail. *Hum Genet* 140:21–42. <https://doi.org/10.1007/s00439-020-02113-x>
- Umer N, Arevalo L, Phadke S, Lohanadan K, Kirfel G, Sons D, Sofia D, Witke W, Schorle H (2021) Loss of profilin3 impairs spermiogenesis by affecting acrosome biogenesis autophagy manchette development and mitochondrial organization. *Front Cell Dev Biol*. <https://doi.org/10.3389/fcell.2021.749559>
- Vander BM, Wyns C (2018) Fertility and infertility: definition and epidemiology. *Clin Biochem* 62:2–10. <https://doi.org/10.1016/j.clinbiochem.2018.03.012>
- Weng M, Sha Y, Zeng YU, Huang N, Liu W, Zhang X, Zhou H (2021) Mutations in DNAH8 contribute to multiple morphological abnormalities of sperm flagella and male infertility. *Acta Biochim Biophys Sin (shanghai)* 53:472–480. <https://doi.org/10.1093/abbs/gmab013>
- WHO (2021) WHO laboratory manual for the examination and processing of human semen, 6th edn. WHO, Geneva
- Wu H, Li W, He X, Liu C, Fang Y, Zhu F, Jiang H, Liu W, Song B, Wang X, Zhou P, Wei Z, Zhang F, Cao Y (2019) Novel CFAP43 and CFAP44 mutations cause male infertility with multiple morphological abnormalities of the sperm flagella (MMAF). *Reprod Biomed Online* 38:769–778. <https://doi.org/10.1016/j.rbmo.2018.12.037>
- Wu T, Hu E, Xu S, Chen M, Guo P, Dai Z, Feng T, Zhou L, Tang W, Zhan L, Fu X, Liu S, Bo X, Yu G (2021) Clusterprofiler 4.0: A universal enrichment tool for interpreting omics data. *Innovation (Camb)*. <https://doi.org/10.1016/j.xinn.2021.100141>
- Wu H, Liu Y, Li Y, Li K, Xu C, Gao Y, Lv M, Guo R, Xu Y, Zhou P, Wei Z, Hua R, He X, Cao Y (2023) DNALI1 deficiency causes male infertility with severe asthenozoospermia in humans and mice by disrupting the assembly of the flagellar inner dynein arms and fibrous sheath. *Cell Death Dis* 14:127. <https://doi.org/10.1038/s41419-023-05653-y>
- Xu K, Yang L, Zhang L, Qi H (2020) Lack of AKAP3 disrupts integrity of the subcellular structure and proteome of mouse sperm and causes male sterility. *Development*. <https://doi.org/10.1242/dev.181057>
- Yu G, Wang LG, Han Y, He QY (2012) Clusterprofiler: an R package for comparing biological themes among gene clusters. *OMICS* 16:284–287. <https://doi.org/10.1089/omi.2011.0118>
- Zhang X, Chen M, Yu R, Liu B, Tian Z, Liu S (2016) FSCB phosphorylation regulates mouse spermatozoa capacitation through suppressing SUMOylation of ROPN1/ROPN1L. *Am J Transl Res* 8:2776–2782
- Zhang J, Xue H, Qiu F, Zhong J, Su J (2019) Testicular spermatozoon is superior to ejaculated spermatozoon for intracytoplasmic sperm injection to achieve pregnancy in infertile males with high sperm DNA damage. *Andrologia*. <https://doi.org/10.1111/and.13175>
- Zhang P, Jiang W, Luo N, Zhu W, Fan L (2019b) IQ motif containing D (IQCD), a new acrosomal protein involved in the acrosome reaction and fertilisation. *Reprod Fertil Dev* 31:898–914. <https://doi.org/10.1071/RD18416>
- Zhang B, Ma H, Khan T, Ma A, Li T, Zhang H, Gao J, Zhou J, Li Y, Yu C, Bao J, Ali A, Murtaza G, Yin H, Gao Q, Jiang X, Zhang F, Liu C, Khan I, Zubair M, Hussain H, Khan R, Yousaf A, Yuan L, Lu Y, Xu X, Wang Y, Tao Q, Hao Q, Fang H, Cheng H, Zhang Y, Shi Q (2020) A DNAH17 missense variant causes flagella destabilization and asthenozoospermia. *J Exp Med*. <https://doi.org/10.1084/jem.20182365>
- Zhang L, Li Y, Huang Y, Li Z (2021) Successful birth after ICSI with testicular immotile spermatozoa from a patient with total MMAF in the ejaculates: a case report. *Zygote*. <https://doi.org/10.1017/S096719942100068X>
- Zhao Y, Wang Y, Guo F, Lu B, Sun J, Wang J, Ren Z (2021) iTRAQ-based proteomic analysis of sperm reveals candidate proteins that affect the quality of spermatozoa from boars on plateaus. *Proteome Sci* 19:9. <https://doi.org/10.1186/s12953-021-00177-9>

Publisher's Note Springer Nature remains neutral with regard to jurisdictional claims in published maps and institutional affiliations.

Springer Nature or its licensor (e.g. a society or other partner) holds exclusive rights to this article under a publishing agreement with the author(s) or other rightsholder(s); author self-archiving of the accepted manuscript version of this article is solely governed by the terms of such publishing agreement and applicable law.